Food Chemistry: X 24 (2024) 101801

Contents lists available at ScienceDirect

Food Chemistry: X

journal homepage: www.sciencedirect.com/journal/food-chemistry-x

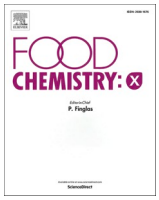

A ratiometric fluorescent electrospun film with high amine sensitivity and stability for visual monitoring of livestock meat freshness

Xiaodong Zhai [a,b,c], Yuhong Xue [a,b], Wenjun Song [a,b], Yue Sun [a], Tingting Shen [a], Xinai Zhang [a], Yanxiao Li [a], Fuyuan Ding [a], Di Zhang [a], Chenguang Zhou [a], Muhammad Arslan [a], Haroon E. Tahir [a], Zhihua Li [a,b], Jiyong Shi [a,b], Xiaowei Huang [a,b,*], Xiaobo Zou [a,b,*]

[a] School of Food and Biological Engineering, Jiangsu University, 301 Xuefu Road, Zhenjiang 212013, China.
[b] Jiangsu Jicui Future Food Technology Research Institute, Yixing 214200, China
[c] Institute of Modern Agriculture and Health Care Industry, Wencheng, 325300, China

ARTICLE INFO

Keywords:
Ratiometric fluorescent film
Electrospinning
Freshness
Beef
Pork
Intelligent packaging

ABSTRACT

Ratiometric fluorescent films with high amine sensitivity and stability were developed to monitor the freshness of beef and pork. Fluorescein isothiocyanate (FITC) and red carbon quantum dots (R-CQD) were used as the amine-responsive indicator and internal reference, respectively. The electrospun films prepared by immobilizing FITC and R-CQD complex (F-R) into polyvinylidene fluoride (PVDF) under 35 %, 55 % and 75 % of relative humidity (RH) were named F-R@PVDF-1, F-R@PVDF-2 and F-R@PVDF-3, respectively. In comparison, the F-R@PVDF-2 film exhibited the highest sensitivity to trimethylamine (TMA), demonstrating a limit of detection (*LOD*) value of 1.59 μM, and meanwhile high stability during storage with Δ*E* value of 1.99 after 14 days of storage at 4 °C. The F-R@PVDF-2 film also showed a significant fluorescent red-to-brown color change during meat freshness monitoring at 4 °C. Conclusively, this study reported a new ratiometric fluorescent film that can be used to track the freshness of meats in food packaging.

1. Introduction

Humans rely on livestock meat as a major source of high-quality protein, high-quality fat, minerals and other nutrients for daily use. However, livestock meats are prone to microbial contamination during production, transportation, sales and other intermediate links. Volatile biogenic amines are produced by decarboxylation of amino acids and amination of carbonyl organic compounds, which can be utilized as a freshness indicator for meats (Siripongpreda, Siralertmukul, & Rodthongkum, 2020; Vasconcelos et al., 2021). Therefore, the detection of biogenic amines is crucial for monitoring the freshness of livestock meats.

Optical sensors have attracted more and more attention because of their high sensitivity, quick response time, and ease of use. They have demonstrated significant promise in the evaluation food quality and safety assessment (Jeon et al., 2020; Liu et al., 2024; Zhan et al., 2021). Nowadays, a variety of fluorescent and visible light sensors based on the response of dyes and pigments to volatile biogenic amines have been developed to monitor freshness of protein-rich foods in intelligent food packaging systems (Alizadeh Sani et al., 2024; Ma et al., 2021; Pirsa, Sani, & Mirtalebi, 2022; Shi et al., 2023). However, some fluorescent sensors among these reported optical sensors generally displayed a single fluorescence intensity change, making it difficult to observe weak changes of fluorescence with the naked eye (Lin, Zhang, Huang, & Li, 2024; Wang, Yu, Zhao, Lu, & Wang, 2021; Zhang, Wang, Xu, Shi, & Yang, 2022). The dual-emission ratiometric fluorescence sensors could provide better applicability due to their high signal-to-noise ratio and automatic calibration ability than single-emission fluorescent sensors (Li et al., 2020; Song et al., 2024). Moreover, dual-emission fluorescent sensors with multiple color changes are more conducive to visual observation (Shen, Wei, Zhu, Cao, & Han, 2022). Recently, there has been a lot of focus on developing ratiometric fluorescence sensors for freshness monitoring of protein-rich foods by using fluorescent nanoprobes, such as silver and gold nanoclusters (Zhang et al., 2022), N, S-carbon dots and CdTe quantum dots (Yan et al., 2022).

Electrospinning is a simple, versatile, and low-cost emerging technique to produce nanofibers. Electrospun films generally have porous structures and high specific surface areas, making them useful for gas

* Corresponding authors at: School of Food and Biological Engineering, Jiangsu University, 301 Xuefu Road, Zhenjiang 212013, China
E-mail addresses: huangxiaowei@ujs.edu.cn (X. Huang), zou_xiaobo@163.com (X. Zou).

https://doi.org/10.1016/j.fochx.2024.101801
Received 2 July 2024; Received in revised form 2 August 2024; Accepted 31 August 2024
Available online 2 September 2024

sensing. Hence, electrospun films with good gas sensitivity have been developed to monitor food freshness (Goudarzi, Moshtaghi, & Shahbazi, 2023; Liu et al., 2023; Pereira, de Sousa Picciani, Calado, & Tonon, 2023; Rezaei, Tajik, & Shahbazi, 2023; Wu et al., 2024). For example, an amine-sensitive ratiometric fluorescent film was constructed by mean of electrospinning method using isothiocyanate, protoporphyrin IX and cellulose, and its fluorescence color changed from red to yellow-green during the storage of shrimp and crab (Jia et al., 2019).

Fluorescein isothiocyanate (FITC) exhibits green color fluorescence with high quantum yield, pH sensitivity, good stability and biocompatibility. Recent studies demonstrated the promising potential of using FITC-based film to monitor shrimp freshness (Quan et al., 2021; Yang, Ding, Li, & Han, 2024). Metal-free carbon quantum dots (CQD) have received considerable attention in food safety area, due to their unique optical properties, high stability, water solubility, promising biocompatibility, and functional properties without cytotoxicity (Khan, Ezati, Kim, & Rhim, 2023). CQD with diverse fluorescent colors have been widely synthesized (Yang et al., 2023). Given that green color contrasts sharply with the red color-possibly the sharpest contrast (Zhang et al., 2013), in this study, we aimed to develop a new ratiometric fluorescent sensor with high color visibility by using green fluorescent FITC and red fluorescent carbon quantum dots (R-CQD). Herein, FITC and R-CQD were served as amin-responsive indicator and internal reference, respectively. Subsequently, the FITC and R-CQD composite (F-R) fluorescent probe was dispersed in polyvinylidene fluoride (PVDF) film by electrospinning method to form hydrophobic and porous films. The effect of different relative humidity (RH) on the gas sensing ability and stability of the electrospun films were also investigated, since environmental humidity is one of the most important factors for the fiber morphology during electrospinning process. Finally, the feasibility of using fabricated ratiometric fluorescent electrospun film in food packaging system to monitor livestock meats (beef and pork) were investigated.

2. Materials and methods

2.1. Materials and reagents

Fresh beef (tenderloin) and pork (tenderloin) were purchased from Jimailong supermarket markets (Zhenjiang, China). Neutral red was purchased from Aladdin Biochemical Technology Co., Ltd. (Shanghai, China). *N*, *N*-Dimethylformamide (DMF), boric acid and magnesium oxide were purchased from Yien Chemical Technology Co., Ltd. (Shanghai, China). Other chemicals, including citric acid monohydrate, PVDF, acetone, hydrochloric acid and TMA solution were purchased from Sinopharm Chemical Reagent Co., Ltd. (Shanghai, China).

2.2. Synthesis of R-CQD

Firstly, R-CQD was synthesized using neutral red and citric acid through hydrothermal method under high pressure as reported in a previous study with a slight modification (Gao et al., 2018). A 2.1 g of citric acid monohydrate was added to 10 mL of ultra-pure water and magnetically stirred for 5 min for sufficient dissolution. Thereafter, 2.9 mg of neutral red powder was added under constant, stirring to obtain a molar ratio of citric acid monohydrate to neutral red of 1000:1. Then, the citric acid monohydrate and neutral red mixture was transferred to a 30 mL of Teflon reactor and heated at 180 °C for 3 h to form R-CQD solution. The obtained R-CQD solution was centrifuged at 11000 rpm for 15 min, and the supernatant was further filtered by using a microporous filter membrane with a pore size of 0.22 μm. Finally, the filtrate was dried by freeze-drying to obtain R-CQD powder.

The relative quantum yield (QY) of R-CQD was measured by using quinine sulfate (QS) as the standard. Firstly, quinine sulfate was dissolved into a 0.1 M of H_2SO_4 aqueous solution to obtain quinine sulfate solutions with different concentrations. At the same time, different concentrations of R-CQD solution were prepared by dispersing R-CQD powder to water. The absorbance values of R-CQD and quinine sulfate solutions were determined by mean of UV–Vis spectrophotometer (Agilent CARY 100, Varian Corporation, USA) to ensure that the absorbance value was less than 0.1. The fluorescence emission spectrum (excitation wavelength is 360 nm) was scanned by a fluorescence spectrophotometer (F98, Prismatic Technology, China), and the curve integration (peak area) of R-CQD and quinine sulfate solution was calculated. Finally, the curve was drawn with the absorbance as the horizontal coordinate and the fluorescence peak area as the vertical coordinate.

The relative quantum yield (QY) of R-CQD was calculated using the following expression:

$$\varphi_x = \varphi_{Qs}\left(\frac{Grad_x}{Grad_{Qs}}\right)\left(\frac{\eta_x^2}{\eta_{Qs}^2}\right) \quad (1)$$

where, φ_x is the relative quantum yield of R-CQDs, φ_{Qs} is the relative quantum yield of quinine sulfate, which is 0.54, and $Grad_x$ and $Grad_{Qs}$ are the slopes of R-CQD and quinine sulfate linear equations, respectively. η_x and η_{Qs} are the refractive indices of R-CQD and quinine sulfate solutions respectively (Both 1.33).

2.3. Construction of R-CQD@FITC probe

Firstly, R-CQD powder was dissolved in water using ultrasonication to obtain a concentration of 1 mg/mL. Then, various R-CQD@FITC ratio fluorescent probes were constructed by mixing 1 mL of R-CQD solution with 40 μL of FITC solution with different concentrations to make that the mass ratios of R-CQD: FITC were 2000:1, 1000:1, 500:1, 333:1, 250:1 and 200:1, respectively. To determine the optimal volume ratio between R-CQD solution and FITC solution, R-CQD@FITC solutions were mixed evenly with 150 μL of 1 M TMA solution for 3 min reaction. The fluorescence spectra of R-CQD@FITC before and after the reaction were recorded by means of fluorescence spectrophotometer.

2.4. Preparation of electrospinning fluorescent films

Firstly, 1.5 g of PVDF powder was added to 10 mL of a mixed solvent (acetone: DMF = 1:4, V/V) and stirred magnetically at 40 °C for 3 h to form a clear solution. The optimized R-CQD@FITC solution was added to PVDF solution under stirring for 30 min, followed with ultrasonic treatment for 30 min to remove bubbles. The obtained solution was inhaled into a disposable syringe using metal needles (inner diameter of 0.84 mm). The positive and negative voltage of the electrospinning machine were set to 15 and − 3 kV, respectively. The internal ambient temperature of the spinning machine was set to 35 °C, and ambient RH was set to 35 %, 55 % and 75 %. The distance between the syringe and receiver was adjusted to 20 cm. Afterwards, the flow rate of the solution was set to 0.001 mm/s and the receiver was controlled to run at 50 r/min. The surface of the receiver was covered with a silicone oil paper. The fluorescent films fabricated under the RH of 35 %, 55 % and 75 % were named as F-R@PVDF-1, F-R@PVDF-2 and F-R@PVDF-3, respectively. Blank PVDF solution for electrospinning was prepared by dissolving 1.5 g of PVDF powder in 10 mL of solvent (acetone: DMF = 1:4, V/V), 40 μL of ethanol, and 1 mL of water.

2.5. Determination of color stability of the films

The fluorescent films were stored in an incubator at 4 °C and their fluorescent images were captured every 24 h by using a digital camera in a UV box (Excitation wavelength:365 nm). The L^* (lightness), a^* (red-to-green) and b^* (blue-to-yellow) values of the images were collected using the image processing software developed by our research group. Parallel experiments were conducted for 3 times, and the average value was taken as the result. The total color difference (ΔE) was calculated by

using the following equation:

$$\Delta E = \sqrt{(\Delta L^*)^2 + (\Delta a^*)^2 + (\Delta b^*)^2} \quad (2)$$

where $\Delta L^* = L^* - L_0^*$, $\Delta a = a^* - a_0^*$, $\Delta b = b^* - b_0^*$; L^*, a^* and b^* are the color parameter of the films after a certain storage time; and L_0^*, a_0^*, and b_0^* are the initial color parameters of the films.

2.6. Determination of sensitivity of the films to trimethylamine (TMA)

Fluorescent films (1 × 1 cm) were adhered to the top of a reaction chamber with 25 °C and 75 % RH for an hour to reach equilibrium. Then, a drop of TMA solution was injected into the closed laboratory and left for an hour to make sure the complete reaction between fluorescent films and TMA. The L^*, a^* and b^* values of fluorescent films were also obtained using the digital camera in a UV box (Excitation wavelength: 365 nm). The concentration of TMA in the chamber was calculated by the following expression:

$$C = \frac{W_S\, V_S\, \rho_S}{M\, V} \quad (3)$$

where C (mol/L) is the concentration of TMA in the reaction chamber; ρ_s is the density of TMA solution (g/mL); V_s is the volume of TMA solution (mL); W_s is the mass fraction of TMA in solution. M is the molar mass of TMA (g/mol); and V is the volume of reaction chamber (L).

The limit of detection (LOD) values of the fluorescent films to TMA can be calculated by the following equation:

$$LOD = 3\sigma/N \quad (4)$$

where σ is the standard deviation of the 13 repeated blank measurements and N is the absolute value of the slope of the calibration curve.

The influence of different humidity on the sensing ability of fluorescent films was also determined. Firstly, reaction chambers with different relative humidity were prepared using $MgCl_2$ saturated solution (30 % RH), NaBr saturated solution (60 % RH), and $ZnSO_4$ saturated solution (90 % RH). F-R@PVDF-2 film was adhered to the top of reaction chambers for an hour to reach equilibrium. Then, a drop of TMA solution was injected to the chamber to obtain a final gas concentration of 400 μM. The total color difference (ΔE) of F-R@PVDF-2 film before and after reaction was calculated.

2.7. Characterization of films

The microstructures of films were observed by using scanning electron microscopy (SEM) and confocal laser scanning microscopy (CLSM). For SEM observation, a small piece of film after drying was pasted onto objective table with conductive glue, followed by a 5 min of gold-spray treatment. The diameter of electrospun fiber of the films was analyzed by using Nano Measurer software. For CLSM observation, a piece of film was placed in the center of glass slide, and covered with a coverslip. The sample was observed with the help of cedar oil. The excitation wavelength of the CLSM was set to 488 nm.

The hydrophobicity of the films was determined to their water contact angle (WCA). The films (20 × 20 mm) were evenly affixed to a glass slide, and the slide was placed on the horizontal work table. When a drop of distilled water was dropped onto the sample surface, the high-speed camera was used to continuously capture the image of water droplets.

2.8. Application in meat freshness monitoring

A piece of 90 g of fresh beef (tenderloin) and pork (tenderloin) were placed in plastic petri dishes (diameter of 9 cm) and F-R@PVDF-2 film (2 × 1 cm) attached to the lids. The petri dishes were sealed with vaseline and stored in a refrigerator at 4 °C. The fluorescence images of the films in a UV box were captured by using a digital camera every 24 h for 6 days.

The total volatile basic nitrogen (TVB-N) content of beef and pork were determined by an automatic Kjeldahl apparatus (Chinese standard GB 5009.228–2016). Briefly, 50 g of meat sample was diced into small pieces through a meat grinder. Then, 10 g of the diced sample was added to 75 mL of distilled water for further homogenization. The mixture was filtered using filter paper and the filtrate was then transferred to a distillation tube containing 1 g of MgO powder. The distillation tube was placed onto the automatic Kjeldahl apparatus, and TVB-N gases were blown by water vapor and finally absorbed by using 30 mL of boric acid (20 g/L). The boric acid solution was titrated with 0.1 M HCl solution by automatic acid-base titrator. In the control group, 75 mL of distilled water without diced meat sample were used. The content of *TVB-N* was calculated according to the amount of 0.1 M HCl used in the titration process by using the following equation:

$$X = \frac{(V_1 - V_2) \times C \times 14}{m} \times 100 \quad (5)$$

where X is the content of *TVB-N* in meat (mg/100 g); C is the concentration of HCl (mol/L); m is the weight of the meat sample (g); V_1 is the volume of 0.1 M HCl used in the process of sample titration (mL); and V_2 is the volume of HCl used in the control group (mL).

2.9. Statistical analysis

All experiments were repeated triplicate to calculate their average values. A one-way analysis of variance (ANOVA) followed by Duncan's multiple range test was used to separate the significant differences ($P < 0.05$) between groups.

3. Results and discussion

3.1. Optimization of R-CQD synthesis conditions

R-CQD was synthesized by one-step hydrothermal method. The synthesis temperature and time are important factors affecting the fluorescence intensity of carbon quantum dots. As shown in **Fig. S1A**, when the synthesis temperature was fixed at 180 °C, the fluorescence intensity of R-CQD gradually increased to the maximum after 3 h of synthesis time, indicating highest QY. Then, the fluorescence intensity of R-CQD gradually decreased with the increase of synthesis time. This may be because that R-CQD was further dehydrated and carbonized, and the overlap of electron clouds between R-CQD led to electron transition, making the fluorescence quench of R-CQD (Xia, Zhu, Feng, Yang, & Yang, 2019). Evidently from **Fig. S1B**, the fluorescence intensity of R-CQD gradually increased when the heating temperature increased from 140 °C to 180 °C and then decreased at higher temperature, under a synthesis time of 3 h. This was most likely caused by R-CQD being over-carbonized at temperatures higher than 180 °C, which made their tiny size effect less noticeable, and led to a decrease in fluorescence intensity. Therefore, the optimum synthesis condition of R-CQD was 180 °C for 3 h. **Fig. S1C** shows the fitting curve of the fluorescence curve integral and absorbance relationship of R-CQD and QS. The QY of R-CQD was calculated to be 26.77 %.

3.2. Characterization of R-CQD

The morphology and particle size of the prepared R-CQD were investigated using transmission electron microscopy (TEM). As shown in Fig. 1A, R-CQD presented a spherical morphology, and the carbon nanoparticles are highly dispersed and homogeneous with an average particle size of 2.48 nm (Fig. 1C), which was consistent with the fact that CQD generally has small size. The HRTEM image exhibited a clear lattice structure with a lattice spacing of 0.21 nm which was similar to the

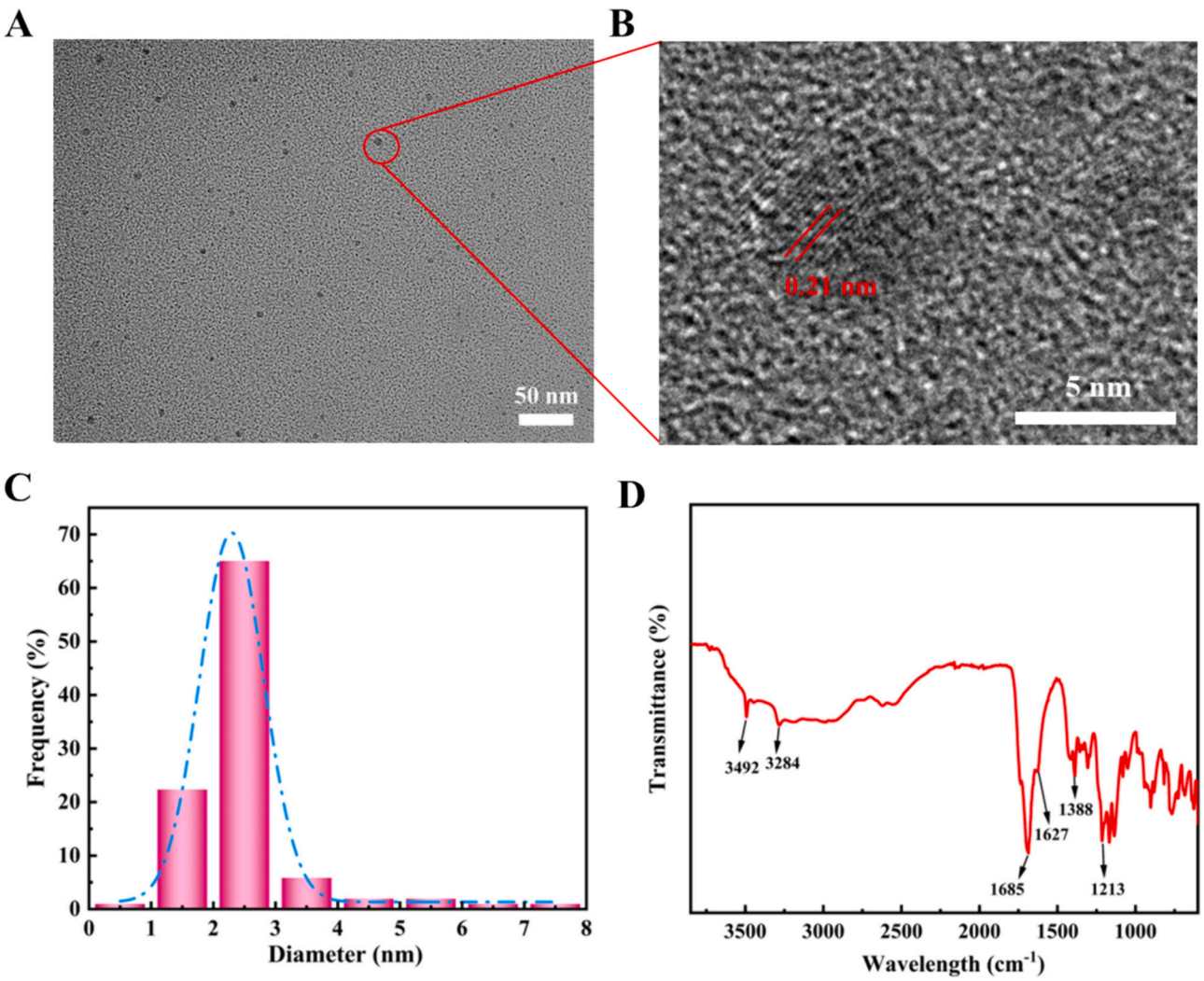

Fig. 1. (A) TEM, (B) HRTEM images, and (C) particle size distribution of the R-CQD; and (D) FTIR spectrum of R-CQD.

(100) facet of graphitic carbon (Fig. 1B) (Si et al., 2018). Fig. 1D showed the FTIR spectrum of the R-CQD. The characteristic peak at 3492 cm^{-1} coincided with the typical stretching vibration of the hydroxyl group (Song et al., 2024). The absorption peak at 1685 cm^{-1} corresponded to the stretching vibration of C═O (Liu et al., 2015). Likewise, absorption peak at 1213 cm^{-1} was attributed to the stretching vibration of C-O-C, suggesting that the R-CQD was rich in oxygen-containing groups (Shangguan et al., 2016). In addition, the characteristic absorption peaks at 1627 cm^{-1} and 1388 cm^{-1} correspond to C═C and C—N, respectively (Liu et al., 2017). The absorption peak at 3284 cm^{-1} was caused by N—H tensile vibration (Qu et al., 2016). Citric acid acted as the main carbon donator of R-CQD and neutral red provided nitrogen source. These findings indicated a successful doping of nitrogen elements into R-CQD.

The functional groups on the surface of R-CQD were further studied using X-ray photoelectron spectroscopy (XPS). As reported in **Fig. S2A**, the XPS spectrum of R-CQDs showed three distinct peaks at 285.08, 399.08 and 532.08 eV, which were attributed to C1s, N1s, and O1s, respectively. It could be seen that R-CQD was composed of three elements: carbon, nitrogen and oxygen. Among them, O element accounts for the largest proportion of 53.88 % followed by C element (44.14 %) and N element (1.98 %). The high-resolution C1s spectrum (**Fig. S2B**) could be further decomposed into three carbon states at 284.78 eV, 286.68 eV and 288.88 eV. The characteristic peak at 288.88 eV corresponded to C—O and C—N bonds. The characteristic peak at 286.68 eV was attributed to the C═O bond. The characteristic peak at 284.78 eV corresponded to the C═C and C—C bonds, which might generate a series of emission wells between the π and π* states of C═C (Liu, Pang, Xu, & Zhang, 2016). **Fig. S2C** shows that the O1s spectrum could also be divided into three components at 531.98 eV, 533.28 eV, and 532.28 eV, which were related to C—O, C═O, and C-OH/C-O-C, respectively (Gao et al., 2018). Peaks at 399.28 eV and 401.48 eV in **Fig. S2D** indicated that nitrogen primarily existed in the form of C—N and N—H bonds (Song et al., 2017), verifying the successful doping of N element in R-CQD.

3.3. *Fluorescence properties of R-CQD and FITC*

Fig. 2A shows the fluorescence emission spectra of R-CQD at different excitation wavelengths. As the excitation wavelength increased from 380 nm to 500 nm, R-CQD reached the maximum emission peak at the excitation wavelength of 470 nm, and the corresponding maximum emission wavelength was 610 nm. Moreover, the wavelength of the emission peak did not change with the excitation wavelength, indicating excitation-independent emission behavior.

FITC reached its maximum fluorescence intensity at an excitation wavelength of 470 nm (Fig. 2B). As the excitation wavelength increased from 400 nm to 500 nm, the emission peak of FITC remained at 519 nm. Fig. 2C-D illustrate the colors presented by R-CQD and FITC under natural light and 365 nm UV light irradiation. R-CQD solution presented

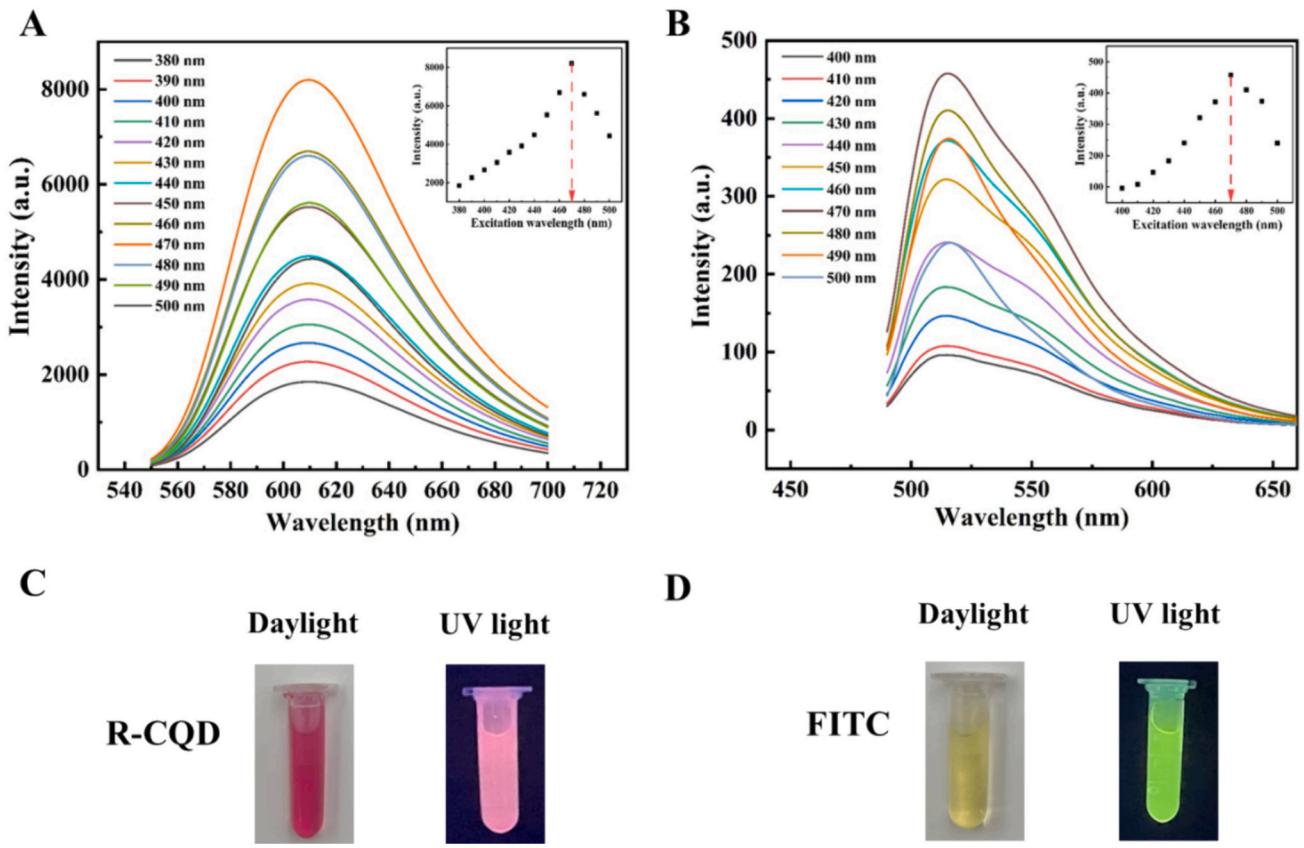

Fig. 2. Fluorescence emission spectra of (A) R-CQD and (B) FITC with excitation of different wavelengths. Photographs of (C) R-CQD and (D) FITC under visible and 365 nm UV light.

red color under both daylight and UV light. FITC displayed yellow color under daylight, while green fluorescence under 365 nm of UV light. R-CQD and FITC could serve as a ratio fluorescent probe R-CQD@FITC, with FITC acting as the TMA-sensitive component of R-CQD@FITC, and R-CQD serving as the internal reference. Since the maximum excitation wavelength for both R-CQD and FITC was 470 nm; therefore, 470 nm was used as the excitation wavelength for R-CQD@FITC ratiometric fluorescent probe.

3.4. Optimization of R-CQD@FITC ratio

Fig. S3 A shows the fluorescent spectra of FITC after reacting with 0–340 μM of TMA. The maximum wavelength was 519 nm and the corresponding fluorescent intensity increased with increasing TMA concentration. A good linear relation was found between the fluorescent intensity at 519 nm and TMA concentration (**Fig. S3B**), indicating that FITC could be used for TMA sensing. In comparison, R-CQD did not show obvious change in maximum wavelength (**Fig. S3C**) and maximum fluorescent intensity (**Fig. S3D**) upon reacting with TMA. Therefore, FITC and R-CQD could be used to construct a ratio fluorescent probe to TMA.

The mass ratio of R-CQD and FITC was optimized to obtain the highest gas sensitivity. Fig. 3A-F show the fluorescent spectra and color of R-CQD@FITC fluorescent probes before and after reaction with TMA. When the mass ratio of R-CQD: FITC was greater than 500:1, the fluorescent color of the solutions after the reaction did not change significantly. This may be due to the insufficient content of FITC in the ratio probe. The color of R-CQD@FITC fluorescent probes after reacting with TMA significantly turned from red to yellow when the mass ratio of R-CQD: FITC was 333:1 or 250:1. However, further increasing FITC content made the original fluorescent color of R-CQD@FITC become yellow, indicating that the change in fluorescent color after reacting with TMA was very weak.

The fluorescent intensity ratio, namely F_{519}/F_{610}, could indicate the intensity of green color in comparison to red color, with a deeper green color when the ratio was higher. It can be seen that the difference values of F_{519}/F_{610} before and after reaction with TMA ($\Delta(F_{519}/F_{610})$), firstly increased and reached the maximum at the mass ratio of 250:1 (R-CQD: FITC) (Fig. 3G), indicating the highest color change. Therefore, the fluorescent probe with a mass ratio of 250:1 (R-CQD: FITC) was utilized for subsequent experiments.

3.5. Response of R-CQD@FITC to TMA solution

Fig. 4A shows the fluorescent spectra of the optimized R-CQD@FITC probe in response to different concentrations of TMA. As the concentration of TMA increased from 0 μM to 340 μM, the emission intensity of the fluorescent probe at 519 nm increased, while the emission intensity at 610 nm remained almost constant. Correspondingly, the fluorescent color of R-CQD@FITC solution changed from red to yellow under a 365 nm UV light (Fig. 4C). Meanwhile, the F_{519}/F_{610} value showed a good linear relationship with TMA concentration in the range of 0 μM to 340 μM, with a correlation coefficient R^2 of 0.9869 (Fig. 4B). Hence, the R-CQD@FITC ratiometric fluorescent probe could be used for TMA sensing.

3.6. Micromorphology of electrospun films

The micromorphology of electrospun film fabricated under different RH was observed using SEM and CLSM. The surface of the blank PVDF electrospun film changed from smooth to rough (Fig. 5A) and the average diameter of the fibers increased from 470 nm to 909 nm with the increase of RH (Fig. 5B). This was probably due to the fact that water vapor as a non-solvent for PVDF would deposit on the PVDF fiber during

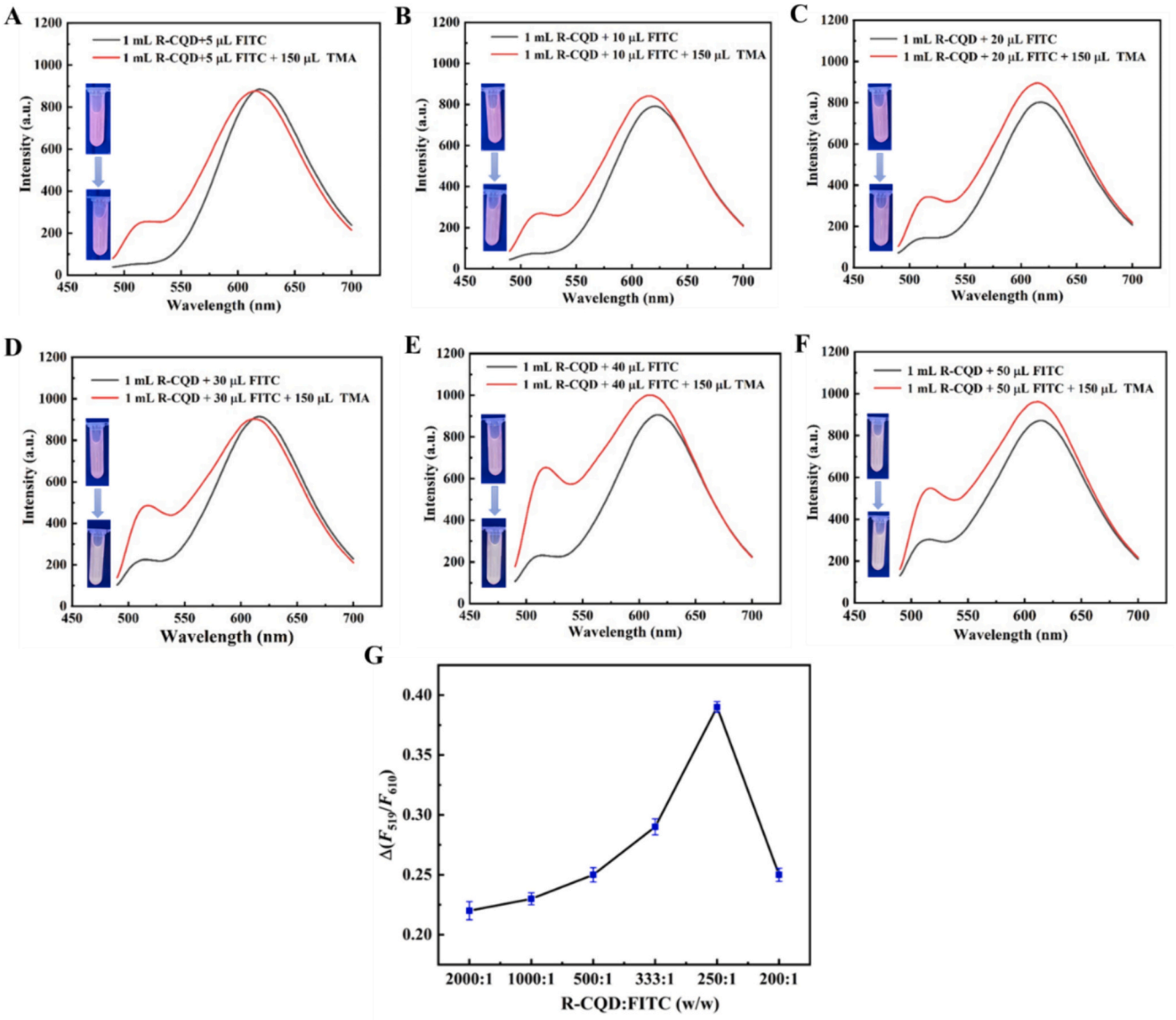

Fig. 3. Fluorescence spectra of R-CQD@FITC probes before and after reaction with TMA, under an excitation wavelength of 470 nm. The mass ratios of R-CQD: FITC were (A) 2000:1, (B) 1000:1, (C) 500:1, (D) 333:1, (E) 250:1 and (F) 200:1, respectively. The insets were fluorescent images of R-CQD@FITC probes before and after reaction. (G) Difference of F_{519}/F_{610} of R-CQD@FITC probes before and after the reaction with TMA.

the evaporation of solvent (acetone and DMF mixture), which led to an increase in fiber diameter and surface roughness (Mailley, Hebraud, & Schlatter, 2021). Similar phenomenon was also observed in roughness (Fig. 5C) and diameter (Fig. 5D) of R-F@PVDF fibers. In comparison, the addition of R-CQD@FITC to PVDF led to an increase of fiber diameter. This could be due to the physical position occupation of R-CQD@FITC within PVDF fibers, and the presence of hydrophilic groups on R-CQD that decreased the evaporation efficiency of the solvent. Moreover, the fibers were severely agglomerated at high RH (75 % RH), which was not beneficial for gas sensing, since that the agglomerated fibers would make the R-CQD@FITC embedded deeply inside of the PVDF polymers, so that the combination between R-CQD@FITC and target gases would be limited to same extent. CLSM images (Fig. 5E) showed the red fluorescence resulting from R-CQD@FITC, and the fluorescence color intensity was nearly equal along the fibers, indicating the uniform dispersion of R-CQD@FITC within PVDF.

3.7. Surface hydrophobicity of electrospun films

The WCA could be used to describe the hydrophilicity/hydrophobicity of the surface of electrospun films. Fig. 6 showed that with the increase of the RH during electrospinning from 35 % to 75 %, the WCA values of the blank PVDF films increased from 117.34° to 142.78°, and the hydrophobicity of the electrospun film gradually increased. This may be due to the increase in the average diameters and surface roughness of the electrospun fibers that reduced the wettability of the fabricated film (Piedrahita, Baba, Quintana, Bardon, & Choquet, 2024). The R-F@PVDF films exhibited lower WCA compared to that of blank PVDF films. This was probably because the surface of R-CQD contained numerous hydrophilic groups such as hydroxyl groups, reducing the hydrophobic characteristics of the electrospun film. However, all of their WCA were still higher than 90°, indicating a hydrophobic surface. Among three R-F@PVDF films, the WCA of R-F@PVDF-3 film presented the highest WCA despite of its uneven micromorphology.

3.8. Self-stability of electrospun films

The fluorescent color stability of the electrospun film has an important influence on the indication accuracy for meat freshness monitoring. **Fig. S4A** shows the fluorescent images of the electrospun

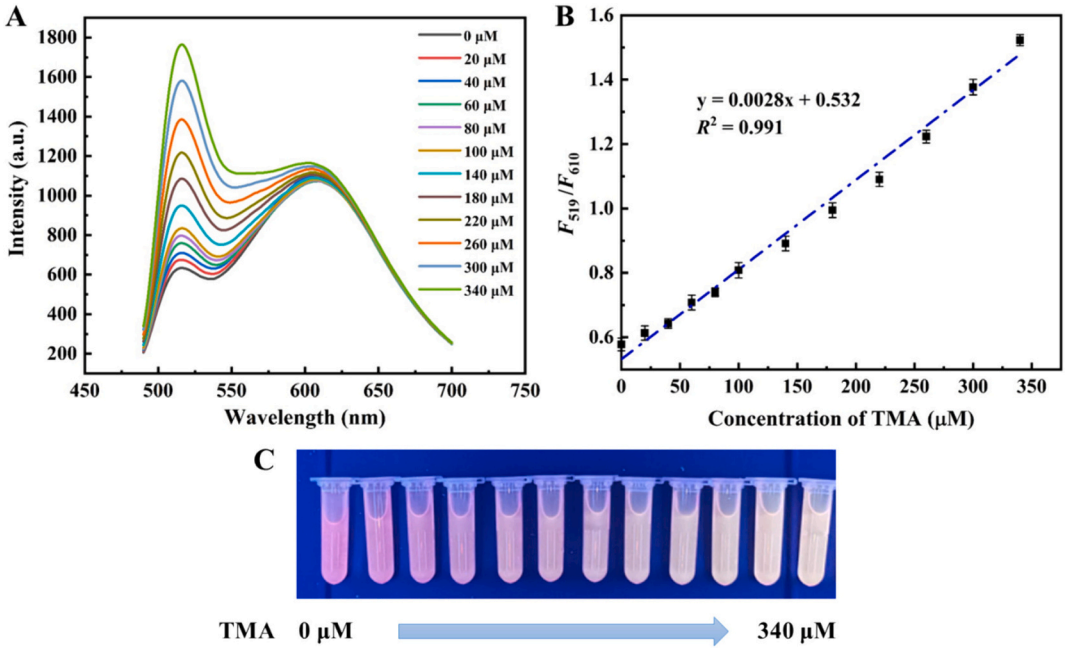

Fig. 4. (A) Fluorescence spectra of R-CQD@FITC fluorescent probe with different concentrations of TMA at a 470 nm excitation, (B) linear relationship between F_{519}/F_{610} and TMA concentration, and (C) the fluorescent images of R-CQD@FITC solutions after reacting with different concentrations of TMA under a 365 nm UV light.

films for 14 d storage under 4 °C. The color changes of F-R@PVDF-1 film and F-R@PVDF-2 film were almost imperceptible, while the fluorescent color of F-R@PVDF-3 film showed a slight fading. In general, the color change $\Delta E < 5$ is considered to be a range of chromaticity that is not easily observed by the naked eye (Zhang et al., 2021). On the 7th day, the ΔE of F-R@PVDF-1, F-R@PVDF-2 and F-R@PVDF-3 film were 1.26, 1.14 and 2.15, respectively, indicating that all three electrospun films have shown good stability within 7 days (**Fig. S4B**). After storage at 4 °C for 14 days, the ΔE values of F-R@PVDF-1 and F-R@PVDF-2 films were 1.87 and 1.99, respectively, while the ΔE value of F-R@PVDF-3 film increased to 6.66. Therefore, the F-R@PVDF-1 and F-R@PVDF-2 film had better stability compared to that of F-R@PVDF-3 film.

3.9. Response of electrospun films to TMA

The responses of the CQD/PVDF and CQD@PVDF film to TMA were evaluated, since TMA is one of the most representative volatile amines during meat spoilage. The fluorescent color response of the F-R@PVDF films to TMA was shown in Fig. 7. As the concentration of TMA increases, the fluorescent color of the electrospun films changed from red to orange, and then to brown. At a certain TMA concentration (150 μM), the color difference ΔE of F-R@PVDF-1 film, F-R@PVDF-2 film and F-R@PVDF-3 film were 21.02, 24.64 and 12.61, respectively, indicating the highest gas sensitivity of F-R@PVDF-2 film. This result could be explained based on their micromorphology as depicted in Fig. 5. The fiber surface of the F-R@PVDF-2 film was rougher with a lot of nanopores as compared to F-R@PVDF-1 film that had very smooth fibers. The rough surface increased the specific surface area of fibers, and nanopores were conducive to the diffusion of TMA into the fibers to combine with FITC. Compared with F-R@PVDF-2 film, the fibers of F-R@PVDF-3 film were severely agglomerated and R-CQD@FITC was largely embedded deeply inside of fibers, reducing the contact area between the fluorescent probes and TMA. The ΔE of F-R@PVDF-2 film and F-R@PVDF-3 film showed linear relationships with TMA concentration in the range of 0–200 μM, 0–150 μM, and 0–300 μM, respectively. According to these linear correction curves, the *LOD* values of F-R@PVDF-1 film, F-R@PVDF-2 film and F-R@PVDF-3 film to TMA were calculated to be 2.52 μM, 1.59 μM and 3.40 μM, respectively, verifying the best gas sensitivity of F-R@PVDF-2 film. **Table S1** shows the linear range and *LOD* of F-R@PVDF-2 film to TMA, compared with other reported works. It can be seen that F-R@PVDF-2 film had good gas sensitivity. The principle of reaction between F-R@PVDF-2 film and TMA was shown in Fig. 7C. The fluorescent intensity of FITC (Green fluorescent color) was enhanced, while that of R-CQD (Red fluorescent color) remained constant, upon reacting with TMA.

In addition, considering that F-R@PVDF-2 film had comparable stability with F-R@PVDF-1 film, therefore, the F-R@PVDF-2 film was used for further application.

3.10. Response of F-R@PVDF-2 film to TMA at different RH

In practical application, the F-R@PVDF-2 film would be fixed in a sealed package containing fresh meats, which would lead to high RH inside of the packaging. Therefore, the effect of RH on the sensing ability of F-R@PVDF-2 film was investigated. As shown in **Fig. S5A**, the fluorescent color of F-R@PVDF-2 film changed from red to orange and then to deep brown after exposure to TMA. The F-R@PVDF-2 film became deep brown at around 160 s, 250 s and 300 s, under the RH of 30 %, 60 % and 90 %, respectively. This resulted indicated that under a higher RH, the reaction between F-R@PVDF-2 film and TMA turned to reach equilibrium more slowly. This could also be seen from the change of ΔE values along with reaction time in **Fig. S5B.** However, the final ΔE values of F-R@PVDF-2 film under different 30 %, 60 % and 90 % RH were 31.5, 30.6 and 30.1, respectively. These results indicated that a higher RH mainly reduced the reaction rate, other than the reaction degree. This could be because that under a high RH, a part of TMA was first combined to water molecules other than directly reaction with FITC, which reduced the reaction rate. But afterwards, TMA concentration in the reaction chamber decreased as consumed by FITC, so that TMA dissolved in water vapor was gradually released from water vapor and then diffused to react with FITC.

3.11. Application of F-R@PVDF-2 film

The F-R@PVDF-2 film exhibited good hydrophobicity, color stability, and sensitivity to TMA, making it suitable for visual monitoring of

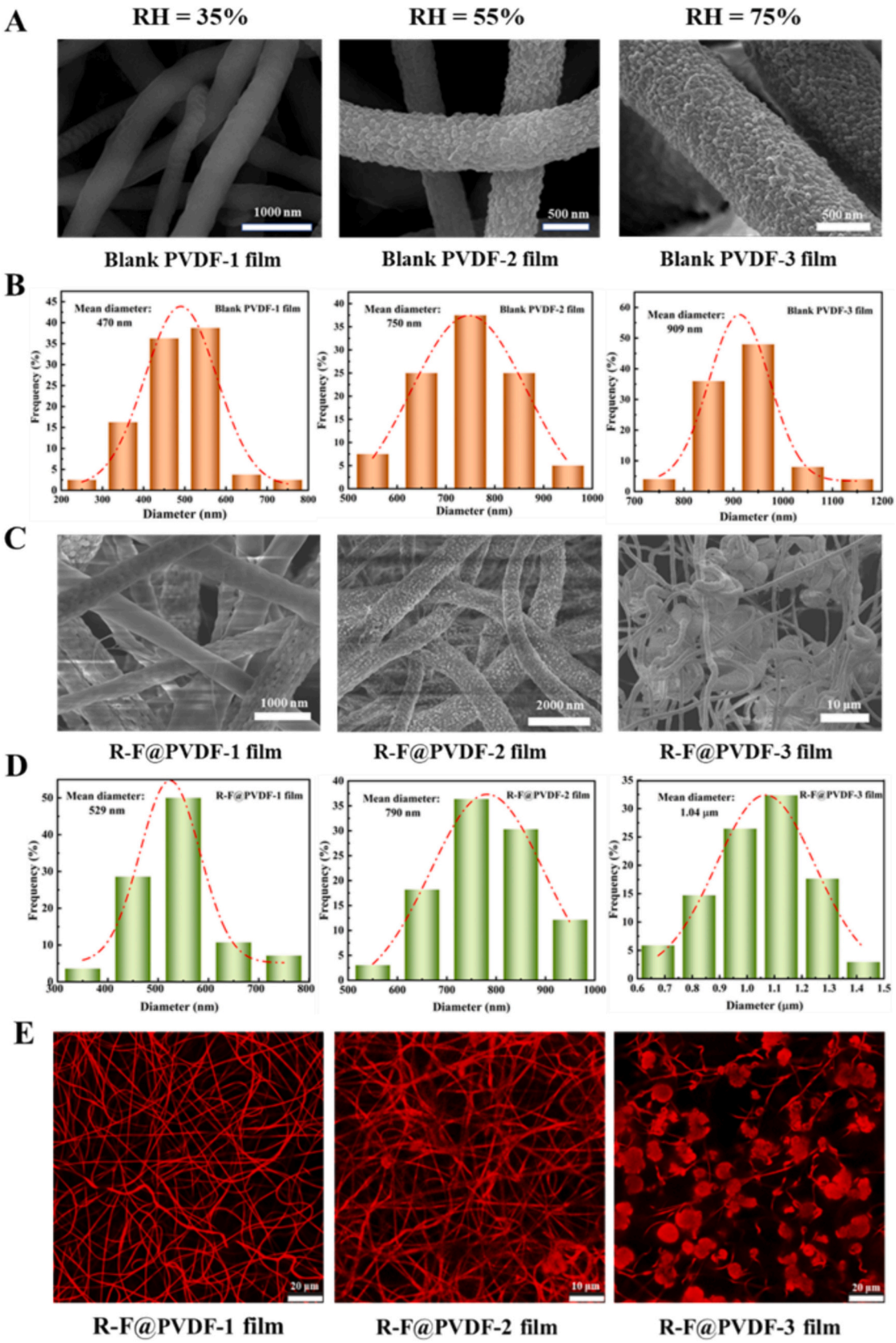

Fig. 5. (A) SEM images and (B) fiber diameter distributions of the blank PVDF films prepared under different RH during electrospinning process. (C) SEM images and (D) fiber diameter distributions of the R-F@PVDF films prepared under different RH during electrospinning process. (E) CLSM images of R-F@PVDF films.

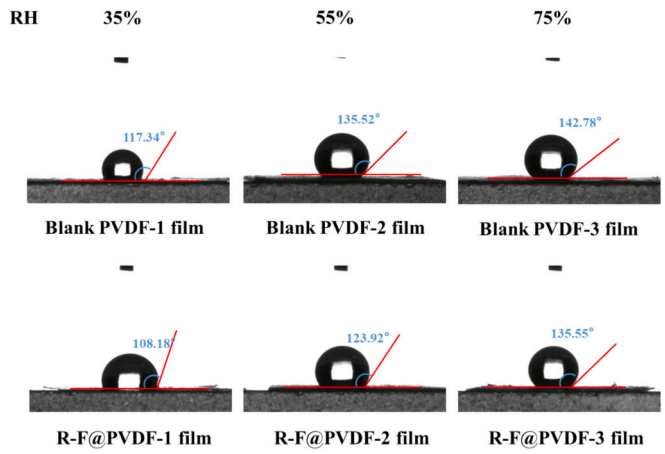

Fig. 6. The WCA images of the blank PVDF films and R-F@PVDF films.

the freshness of beef and pork. Chinese standard was used to determine the freshness of beef and pork based on their *TVB-N* contents. Evidently from Fig. 8A, fluorescent color of F-R@PVDF-2 film gradually turned from red to brown, indicating the reaction between the F-R@PVDF-2 film and volatile gases from meats. *TVB-N* values of beef (Fig. 8B) and pork (Fig. 8C) gradually increased with the storage time. The Chinese standard GB 2707–2016 states that the rejection limits of *TVB-N* level for fresh beef and pork was 15 mg/100 g.

The *TVB-N* content of beef increased from 7.34 mg/100 g to 13.56 mg/100 g at the 4th day, indicating that the beef was still fresh. According to the calibration curve between *TVB-N* content and storage time, the *TVB-N* content of beef reached 15 mg/100 g after nearly 4.4 day. At this point, the ΔE value of F-R@PVDF-2 film was 13.5, indicating this color change was obvious for the naked eye as $\Delta E > 5$. The *TVB-N* of pork increased from 8.45 mg/100 g to 13.85 mg/100 g over 3 days, indicating that the pork was still fresh on the third day. According to the calibration curve between *TVB-N* content and storage time, the *TVB-N* content of pork increased to 15 mg/100 g nearly after 3.7 day, indicating that the pork was not fresh. At this point, the ΔE value of the F-R@PVDF-2 film increased to 9.0, meaning that this color change was evident for the naked eye. As a result, the F-R@PVDF-2 film could realize the visual monitoring of the beef and pork freshness.

4. Conclusion

R-CQD with maximum excitation and emission wavelength of 470 and 610 nm was successfully synthesized. R-CQD and FITC complex with the optimal mass ratio of 1:250 was used as the ratiometric fluorescent probe for TMA. Afterwards, highly hydrophobic fluorescent electrospun films were prepared by immobilizing R-CQD@ FITC into PVDF. During electrospinning process, RH exhibited a significant effect on the micromorphology, hydrophobicity, stability, and gas sensitivity of the films. The F-R@PVDF-2 film prepared at 55 % RH showed good hydrophobicity, stability, and TMA sensitivity with *LOD* to TMA of 1.59 μM. The F-R@PVDF-2 film showed a significant fluorescent color change from red to brown during the visual monitoring of pork and beef freshness at 4 °C. Conclusively, this study presented a new ratiometric fluorescent sensor to monitor meat freshness in intelligent food packaging system.

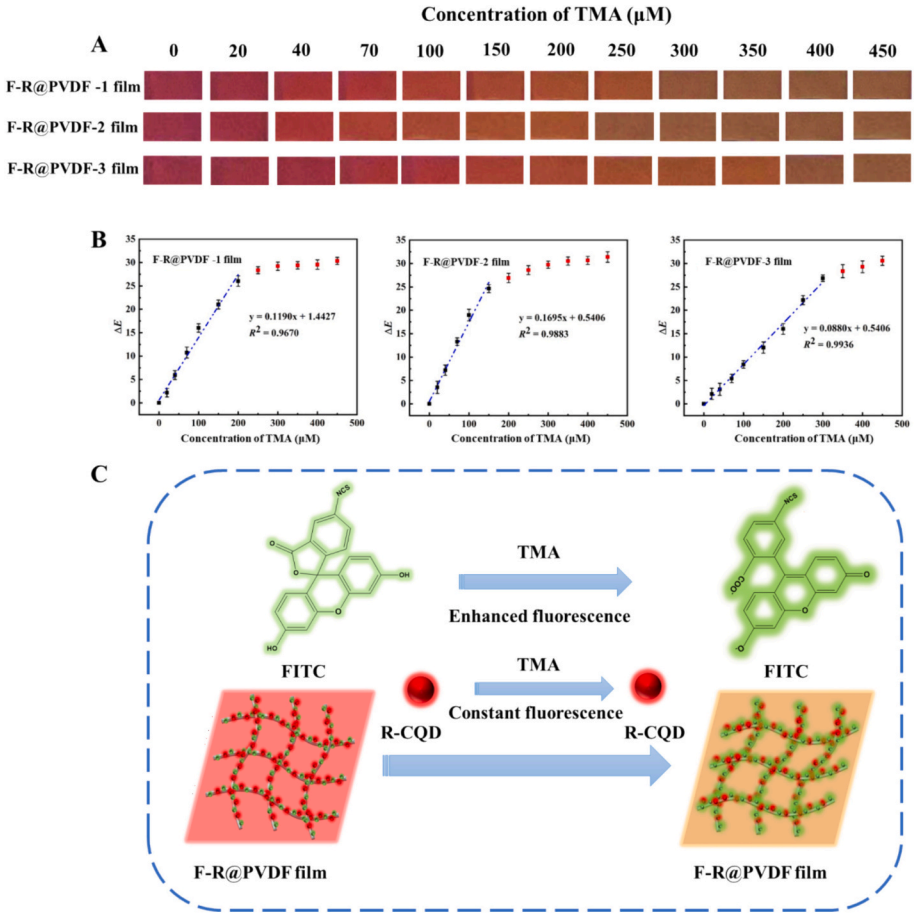

Fig. 7. (A) The fluorescent images of the F-R@PVDF films in response to TMA at different concentrations. (B) The plot of ΔE values of the films versus the concentration of TMA. (C) Principle diagram of TMA and R-CQD@FITC reaction.

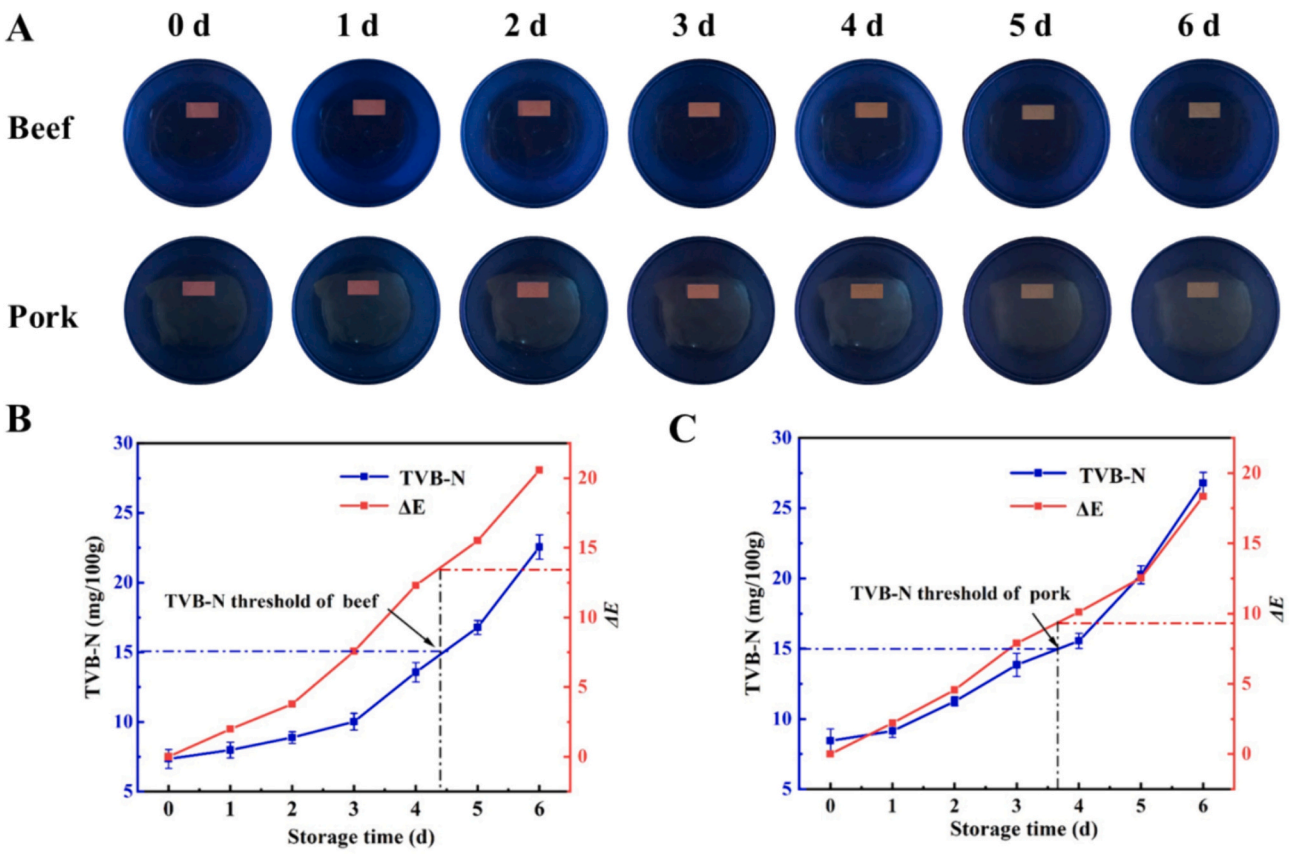

Fig. 8. (A) The fluorescent images of F-R@PVDF-2 film during monitoring the freshness of beef and pork. (B) The changes of TVB-N contents of beef and Δ*E* values of F-R@PVDF-2 film with time. (C) The changes of TVB-N contents of pork and Δ*E* values of F-R@PVDF-2 film with time.

CRediT authorship contribution statement

Xiaodong Zhai: Writing – review & editing, Writing – original draft, Methodology, Investigation, Formal analysis, Data curation, Conceptualization. **Yuhong Xue:** Writing – review & editing, Writing – original draft, Methodology, Investigation, Formal analysis, Conceptualization. **Wenjun Song:** Writing – review & editing, Writing – original draft, Methodology, Investigation, Formal analysis, Conceptualization. **Yue Sun:** Writing – review & editing, Validation, Conceptualization. **Tingting Shen:** Writing – review & editing, Validation, Conceptualization. **Xinai Zhang:** Writing – review & editing, Validation, Conceptualization. **Yanxiao Li:** Writing – review & editing, Validation, Conceptualization. **Fuyuan Ding:** Writing – review & editing, Validation, Conceptualization. **Di Zhang:** Writing – review & editing, Validation, Conceptualization. **Chenguang Zhou:** Writing – review & editing, Validation, Conceptualization. **Muhammad Arslan:** Writing – review & editing, Validation, Conceptualization. **Haroon E. Tahir:** Writing – review & editing, Validation, Conceptualization. **Zhihua Li:** Writing – review & editing, Validation, Supervision, Resources, Funding acquisition, Conceptualization. **Jiyong Shi:** Writing – review & editing, Validation, Conceptualization. **Xiaowei Huang:** Writing – review & editing, Validation, Supervision, Resources, Funding acquisition, Conceptualization. **Xiaobo Zou:** Writing – review & editing, Validation, Supervision, Resources, Funding acquisition, Conceptualization.

Declaration of competing interest

All authors declare that our current study has no conflict of interest.

Data availability

Data will be made available on request.

Acknowledgment

The authors gratefully acknowledge the financial support provided by National Key Research and Development Program of China (2023YFE0105500), National Natural Science Foundation of China (32102080, 32272407, 32372465), Special Funds for Jiangsu Province Science and Technology Plans (BZ2024029), Natural Science Foundation of Jiangsu Province (BK20220111), Earmarked fund for Agriculture Research System of China, and Priority Academic Program Development of Jiangsu Higher Education Institutions.

Appendix A. Supplementary data

Supplementary data to this article can be found online at https://doi.org/10.1016/j.fochx.2024.101801.

References

Alizadeh Sani, M., Zhang, W., Abedini, A., Khezerlou, A., Shariatifar, N., Assadpour, E., … Jafari, S. M. (2024). Intelligent packaging systems for the quality and safety monitoring of meat products: From lab scale to industrialization. *Food Control, 160*, Article 110359. https://doi.org/10.1016/j.foodcont.2024.110359

Gao, W., Song, H., Wang, X., Liu, X., Pang, X., Zhou, Y., Gao, B., & Peng, X. (2018). Carbon dots with red emission for sensing of Pt^{2+}, Au^{3+}, and Pd^{2+} and their bioapplications in vitro and in vivo. *ACS Applied Materials & Interfaces, 10*(1), 1147–1154. https://doi.org/10.1021/acsami.7b16991

Goudarzi, J., Moshtaghi, H., & Shahbazi, Y. (2023). Kappa-carrageenan-poly(vinyl alcohol) electrospun fiber mats encapsulated with Prunus domestica anthocyanins and epigallocatechin gallate to monitor the freshness and enhance the shelf-life

quality of minced beef meat. *Food Packaging and Shelf Life, 35*, Article 101017. https://doi.org/10.1016/j.fpsl.2022.101017

Jeon, S., Kim, T.-I., Jin, H., Lee, U., Bae, J., Bouffard, J., & Kim, Y. (2020). Amine-reactive activated esters of meso-CarboxyBODIPY: Fluorogenic assays and labeling of amines, amino acids, and proteins. *Journal of the American Chemical Society, 142*(20), 9231–9239. https://doi.org/10.1021/jacs.9b13982

Jia, R., Tian, W., Bai, H., Zhang, J., Wang, S., & Zhang, J. (2019). Amine-responsive cellulose-based ratiometric fluorescent materials for real-time and visual detection of shrimp and crab freshness. *Nature Communications, 10*(1), 795. https://doi.org/10.1038/s41467-019-08675-3

Khan, A., Ezati, P., Kim, J. T., & Rhim, J. W. (2023). Biocompatible carbon quantum dots for intelligent sensing in food safety applications: Opportunities and sustainability. *Materials Today Sustainability, 21*, Article 100306. https://doi.org/10.1016/j.mtsust.2022.100306

Li, C., Yang, Q., Wang, X., Arabi, M., Peng, H., Li, J., Xiong, H., & Chen, L. (2020). Facile approach to the synthesis of molecularly imprinted ratiometric fluorescence nanosensor for the visual detection of folic acid. *Food Chemistry, 319*, Article 126575. https://doi.org/10.1016/j.foodchem.2020.126575

Lin, W., Zhang, Y., Huang, J., & Li, Z. (2024). Fluorescence and pectinase double-triggered chitosan/pectin/calcium propionate/curcumin-β-cyclodextrin complex film for pork freshness monitoring and maintenance. *International Journal of Biological Macromolecules, 257*, Article 128603. https://doi.org/10.1016/j.ijbiomac.2023.128603

Liu, J., Wu, D., Wu, Y., Shi, Y., Liu, W., Sun, Z., & Li, G. (2024). Recent advances in optical sensors and probes for the detection of freshness in food samples: A comprehensive review (2020−2023). *TrAC Trends in Analytical Chemistry, 177*, Article 117793. https://doi.org/10.1016/j.trac.2024.117793

Liu, L., Feng, F., Chin Paau, M., Hu, Q., Liu, Y., Chen, Z., … Choi, M. M. F. (2015). Sensitive determination of kaempferol using carbon dots as a fluorescence probe. *Talanta, 144*, 390–397. https://doi.org/10.1016/j.talanta.2015.07.004

Liu, X., Pang, J., Xu, F., & Zhang, X. (2016). Simple approach to synthesize amino-functionalized carbon dots by carbonization of chitosan. *Scientific Reports, 6*(1), 31100. https://doi.org/10.1038/srep31100

Liu, X., Song, X., Gou, D., Li, H., Jiang, L., Yuan, M., & Yuan, M. (2023). A polylactide based multifunctional hydrophobic film for tracking evaluation and maintaining beef freshness by an electrospinning technique. *Food Chemistry, 428*, Article 136784. https://doi.org/10.1016/j.foodchem.2023.136784

Liu, Y., Duan, W., Song, W., Liu, J., Ren, C., Wu, J., Liu, D., & Chen, H. (2017). Red emission B, N, S-co-doped carbon dots for colorimetric and fluorescent dual mode detection of Fe^{3+} ions in complex biological fluids and living cells. *ACS Applied Materials & Interfaces, 9*(14), 12663–12672. https://doi.org/10.1021/acsami.6b15746

Ma, Q., Lu, X., Wang, W., Hubbe, M. A., Liu, Y., Mu, J., … Rojas, O. J. (2021). Recent developments in colorimetric and optical indicators stimulated by volatile base nitrogen to monitor seafood freshness. *Food Packaging and Shelf Life, 28*, Article 100634. https://doi.org/10.1016/j.fpsl.2021.100634

Mailley, D., Hebraud, A., & Schlatter, G. (2021). A review on the impact of humidity during electrospinning: From the nanofiber structure engineering to the applications. *Macromolecular Materials and Engineering, 306*(7), 2100115. https://doi.org/10.1002/mame.202100115

Pereira, P. F. M., de Sousa Picciani, P. H., Calado, V., & Tonon, R. V. (2023). Gelatin-based films and mats as electro-sensoactive layers for monitoring volatile compounds related to meat spoilage. *Food Packaging and Shelf Life, 36*, Article 101049. https://doi.org/10.1016/j.fpsl.2023.101049

Piedrahita, C. R., Baba, K., Quintana, R., Bardon, J., & Choquet, P. (2024). Superhydrophobicity of direct plasma synthesized and deposited thin films: Effect of chemical-induced and substrate roughness. *Applied Surface Science, 159700*. https://doi.org/10.1016/j.apsusc.2024.159700

Pirsa, S., Sani, I. K., & Mirtalebi, S. S. (2022). Nano-biocomposite based color sensors: Investigation of structure, function, and applications in intelligent food packaging. *Food Packaging and Shelf Life, 31*, Article 100789. https://doi.org/10.1016/j.fpsl.2021.100789

Qu, S., Zhou, D., Li, D., Ji, W., Jing, P., Han, D., Liu, L., Zeng, H., & Shen, D. (2016). Toward efficient orange emissive carbon nanodots through conjugated sp (2)-domain controlling and surface charges engineering. *Advanced Materials, 28*(18), 3516–3521. https://doi.org/10.1002/adma.201504891

Quan, Z., He, H., Zhou, H., Liang, Y., Wang, L., Tian, S., Zhu, H., & Wang, S. (2021). Designing an intelligent nanofiber ratiometric fluorescent sensor sensitive to biogenic amines for detecting the freshness of shrimp and pork. *Sensors and Actuators B: Chemical, 333*, Article 129535. https://doi.org/10.1016/j.snb.2021.129535

Rezaei, F., Tajik, H., & Shahbazi, Y. (2023). Intelligent double-layer polymers based on carboxymethyl cellulose-cellulose nanocrystals film and poly(lactic acid)-Viola odorata petal anthocyanins nanofibers to monitor food freshness. *International Journal of Biological Macromolecules, 252*, Article 126512. https://doi.org/10.1016/j.ijbiomac.2023.126512

Shangguan, J., He, D., He, X., Wang, K., Xu, F., Liu, J., Tang, J., Yang, X., & Huang, J. (2016). Label-free carbon-dots-based Ratiometric fluorescence pH Nanoprobes for intracellular pH sensing. *Analytical Chemistry, 88*(15), 7837–7843. https://doi.org/10.1021/acs.analchem.6b01932

Shen, Y., Wei, Y., Zhu, C., Cao, J., & Han, D.-M. (2022). Ratiometric fluorescent signals-driven smartphone-based portable sensors for onsite visual detection of food contaminants. *Coordination Chemistry Reviews, 458*, Article 214442. https://doi.org/10.1016/j.ccr.2022.214442

Shi, S., Xu, X., Feng, J., Ren, Y., Bai, X., & Xia, X. (2023). Preparation of NH_3- and H_2S-sensitive intelligent pH indicator film from sodium alginate/black soybean seed coat anthocyanins and its use in monitoring meat freshness. *Food Packaging and Shelf Life, 35*, Article 100994. https://doi.org/10.1016/j.fpsl.2022.100994

Si, M., Zhang, J., He, Y., Yang, Z., Yan, X., Liu, M., Zhuo, S., Wang, S., Min, X., Gao, C., Chai, L., & Shi, Y. (2018). Synchronous and rapid preparation of lignin nanoparticles and carbon quantum dots from natural lignocellulose. *Green Chemistry, 20*(15), 3414–3419. https://doi.org/10.1039/C8GC00744F

Siripongpreda, T., Siralertmukul, K., & Rodthongkum, N. (2020). Colorimetric sensor and LDI-MS detection of biogenic amines in food spoilage based on porous PLA and graphene oxide. *Food Chemistry, 329*, Article 127165. https://doi.org/10.1016/j.foodchem.2020.127165

Song, W., Zhai, X., Shi, J., Zou, X., Xue, Y., Sun, Y., Sun, W., Zhang, J., Huang, X., Li, Z., Shen, T., Li, Y., Zhou, C., Holmes, M., Gong, Y., & Povey, M. (2024). A ratiometric fluorescence amine sensor based on carbon quantum dot-loaded electrospun polyvinylidene fluoride film for visual monitoring of food freshness. *Food Chemistry, 434*, Article 137423. https://doi.org/10.1016/j.foodchem.2023.137423

Song, Y., Zhu, C., Song, J., Li, H., Du, D., & Lin, Y. (2017). Drug-derived bright and color-tunable N-doped carbon dots for cell imaging and sensitive detection of Fe^{3+} in living cells. *ACS Applied Materials & Interfaces, 9*(8), 7399–7405. https://doi.org/10.1021/acsami.6b13954

Vasconcelos, H., de Almeida, J. M. M. M., Matias, A., Saraiva, C., Jorge, P. A. S., & Coelho, L. C. C. (2021). Detection of biogenic amines in several foods with different sample treatments: An overview. *Trends in Food Science & Technology, 113*, 86–96. https://doi.org/10.1016/j.tifs.2021.04.043

Wang, C., Yu, Z., Zhao, X., Lu, H., & Wang, Q. (2021). Rapid response to amine vapor based on fluorescent light-up sensor for real-time and visual detection of crawfish and fish freshness. *Dyes and Pigments, 189*, Article 109228. https://doi.org/10.1016/j.dyepig.2021.109228

Wu, J.-H., Liao, J.-H., Hu, T.-G., Zong, M.-H., Wen, P., & Wu, H. (2024). Fabrication of multifunctional ethyl cellulose/gelatin-based composite nanofilm for the pork preservation and freshness monitoring. *International Journal of Biological Macromolecules, 265*, Article 130813. https://doi.org/10.1016/j.ijbiomac.2024.130813

Xia, C., Zhu, S., Feng, T., Yang, M., & Yang, B. (2019). Evolution and synthesis of carbon dots: From carbon dots to carbonized polymer dots. *Advanced Science, 6*(23), 1901316. https://doi.org/10.1002/advs.201901316

Yan, J., Fu, Q., Zhang, S., Liu, Y., Shi, X., Hou, J., Duan, J., & Ai, S. (2022). A sensitive ratiometric fluorescent sensor based on carbon dots and CdTe quantum dots for visual detection of biogenic amines in food samples. *Spectrochimica Acta Part A: Molecular and Biomolecular Spectroscopy, 282*, Article 121706. https://doi.org/10.1016/j.saa.2022.121706

Yang, H.-L., Bai, L.-F., Geng, Z.-R., Chen, H., Xu, L.-T., Xie, Y.-C., Wang, D.-J., Gu, H.-W., & Wang, X.-M. (2023). Carbon quantum dots: Preparation, optical properties, and biomedical applications. *Materials Today Advances, 18*, Article 100376. https://doi.org/10.1016/j.mtadv.2023.100376

Yang, S., Ding, Q., Li, Y., & Han, W. (2024). Bacterial cellulose/gelatin-based pH-responsive functional film for food freshness monitoring. *International Journal of Biological Macromolecules, 259*, Article 129203. https://doi.org/10.1016/j.ijbiomac.2024.129203

Zhan, Y., Yang, S., Chen, L., Zeng, Y., Li, L., Lin, Z., Guo, L., & Xu, W. (2021). Ultrahigh efficient FRET Ratiometric fluorescence biosensor for visual detection of alkaline phosphatase activity and its inhibitor. *ACS Sustainable Chemistry & Engineering, 9*(38), 12922–12929. https://doi.org/10.1021/acssuschemeng.1c03830

Zhang, C., Yin, A.-X., Jiang, R., Rong, J., Dong, L., Zhao, T., Sun, L.-D., Wang, J., Chen, X., & Yan, C.-H. (2013). Time–Temperature Indicator for Perishable Products Based on Kinetically Programmable Ag Overgrowth on Au Nanorods. *ACS Nano, 7*(5), 4561–4568. https://doi.org/10.1021/nn401266u

Zhang, J., Huang, X., Shi, J., Liu, L., Zhang, X., Zou, X., Xiao, J., Zhai, X., Zhang, D., Li, Y., & Shen, T. (2021). A visual bi-layer indicator based on roselle anthocyanins with high hydrophobic property for monitoring griskin freshness. *Food Chemistry, 355*, Article 129573. https://doi.org/10.1016/j.foodchem.2021.129573

Zhang, J., Wang, Y., Xu, Z., Shi, C., & Yang, X. (2022). A sensitive fluorescence-visualized sensor based on an InP/ZnS quantum dots-sodium rhodizonate system for monitoring fish freshness. *Food Chemistry, 384*, Article 132521. https://doi.org/10.1016/j.foodchem.2022.132521

Zhang, W., Ma, J., Sun, D.-W., Cheng, J., Wang, Z., & Tang, B. Z. (2022). An improved ratiometric fluorescent tag based on aggregation-induced emission luminogen for in-situ monitoring of seafood freshness. *Sensors and Actuators B: Chemical, 373*, Article 132744. https://doi.org/10.1016/j.snb.2022.132744